Supporting Information for "Role of fluid injection on earthquake size in dynamic rupture simulations on rough faults"

Jeremy Maurer,[1,2] Paul Segall,[1] and Eric M. Dunham[1]

Contents of this file

1. Text S1 to S4

2. Figures S1-S13

3. Tables S1-S5

———

Corresponding author: Jeremy Maurer, Missouri University of Science and Technology (jmaurer@mst.edu)

[1]Department of Geophysics, Stanford

University, Stanford, California, USA

[2]Now in the Geological Engineering

program, Missouri University of Science and

Technology, Rolla, MO, USA.

Text S1: Details of the rupture simulator

Supp. Fig. S1 shows the problem geometry. Full details of the model are given in the papers cited in the main text; here we summarize the governing equations and initial conditions for our simulations. The medium is idealized as a Drucker-Prager elastic-plastic solid, which permits off-fault plastic relaxation of stress at high strains [see *Dunham et al.*, 2011]. Off-fault plasticity is important in the context of rough faults because plastic (i.e., irreversible) strain bounds stresses that with pure elasticity would grow extremely large due to slip on the rough fault.

We use a strong rate-weakening (SRW) friction law in our simulations. Friction obeys ordinary rate-and-state (ORS) friction at low velocities, and transitions to a very weak dynamic friction value (μ_w) above a critical weakening velocity V_W. Steady-state friction is given by:

$$\mu_{ss}(V) = \mu_w + \frac{\mu^{LV} - \mu_w}{[1 + (V/V_W)^n]^{(1/n)}} \tag{1}$$

where V is fault slip rate, the exponent n governs how rapidly the transition from ordinary to weak friction occurs, and μ^{LV} is the conventional low-velocity friction coefficient:

$$\mu^{LV} = \mu_0 - (b - a)\ln(V/V_0).$$

with parameters $\mu_0 = \mu_{ss}(V_0)$, a, b, and V_0 =reference velocity. We use a regularized rate-and-state friction law in the slip law form [*Rice*, 1983; *Noda et al.*, 2009]:

$$\mu^{LV}(V, \Theta) = a\operatorname{arcsinh}\left(\frac{V}{2V_0}e^{\Theta/a}\right) \tag{2}$$

with state Θ (note the difference between Θ used here and θ used in many theoretical papers on ORS friction, they are related by $\Theta = \mu_0 + b\ln(\theta/\theta_0)$). In general we adopt the same parameter values as *Dunham et al.* [2011], who use a fully weakened friction coeffi-

cient of $\mu_w = 0.13$ and weakening velocity $V_W = 0.17$ m/s (see Tables in the Supplemental Material for all parameter values).

FDMAP uses the slip law for state evolution:

$$\frac{d\Theta}{dt} = -\frac{V}{d_c}\left(\mu(V, \Theta) - \mu_{ss}(V)\right) \tag{3}$$

The initial state Θ_{ini} is specified as a constant over the entire fault and the initial velocity on the fault is chosen to be consistent with this value and the locally-resolved stress on the fault. Because stress is heterogeneous for rough faults, the initial velocity is also heterogeneous and for very rough faults can vary over 10 orders of magnitude. Initial velocity in our SRW simulations is always below $V_0 = 10^{-6}$ m/s.

An important parameter in SRW-friction simulations under low stress conditions is τ^{pulse}, defined as the largest shear stress τ_0^b such that

$$\tau_0^b - \frac{G}{2c_s}V \le \sigma_0\mu_{ss}(V)$$

for all $V > 0$, where c_s is the shear wave speed [*Zheng and Rice*, 1998]. For rough faults, this expression is modified to include an additional term due to roughness drag (see below). Dynamic earthquake simulations using a SRW friction law lead to pulse-like ruptures when the background stress is close to τ^{pulse}. Rupture style transitions to crack-like at sufficiently high stress levels. Pulse-like ruptures on rough faults may self-arrest naturally due to fluctuations in the local stress around fault bends, or if the background stress is high enough they may rupture the entire fault. Because dynamic friction is very weak, the background stress required to sustain ruptures (approximately τ^{pulse}) can be much lower than the static frictional strength of the fault.

For initial stresses that are a significant fraction of the static strength, (how large depends on roughness), ruptures grow indefinitely. *Fang and Dunham* [2013] considered background shear/normal stress ratios of 0.28-0.4, much lower than values typically associated with static friction (0.6-0.8). To nucleate an event, stress must still reach static strength (0.7 in our simulations), but once nucleated events can propagate at much lower stress levels. For more details about the model, see references in the main text.

The faults in our simulations are 60 km, which is longer than most induced earthquakes; however, length scales can be normalized using the length of the state evolution region at the rupture tip (R_0) [*Dunham et al.*, 2011, and references therein]:

$$R_0 \approx \frac{3\pi}{4} \frac{G d_c}{\tau^p - \tau^r} \tag{4}$$

for shear modulus G, critical state evolution distance d_c. Peak stress τ^p can be estimated as

$$\tau^p \approx \sigma_0 \left[a \log \left(V^p / V_0 \right) + \Theta_{\mathrm{ini}} \right] \tag{5}$$

and residual stress τ^r is

$$\tau^r \approx \sigma_0 \mu_{ss} \left(V^{\mathrm{pulse}} \right) \tag{6}$$

V^p is the peak velocity at dynamic speeds, approximately 1 m/sec, V^{pulse} is the steady-state velocity at τ^{pulse}, and Θ_{ini} is the initial state on the fault (see Eq. 2 and discussion). For the simulations discussed in this section, $\tau^p - \tau^r \approx 60$ MPa and $d_c \approx 0.05$ m, so R_0 is of order 100 m.

Fault profiles are constructed by filtering zero-mean white noise to have the desired spectral properties and shifting the profile so that the endpoints are located at $y = 0$ and the highest resolved shear/normal stress ratio at wavelengths larger than the approximate

nucleation dimension is at the origin. For our study, this dimension is approximated by L_b:

$$L_b = \frac{G^* d_c}{b \sigma_0} \tag{7}$$

and is about 1.6 km.

Text S2: Diffusion in a medium with a permeable channel

To introduce a finite length scale into the pore pressure diffusion problem, we introduce a high-permeability channel that crosses the domain and the fault (Supp. Fig. S2). The injector is located inside this channel, and pressure diffuses through the channel to the fault. The domain as total length $2L = 60$ km, and total width $L = 30$ km. The length of the channel is $2L_k$.

The governing equations are:

$$\nabla \cdot [D(x) \nabla p] = \frac{\partial p}{\partial t} + \frac{q}{\rho_f \phi \beta} \delta(x) \delta(y - y_0) H(t) \tag{8}$$

for diffusivity $D(x) = \kappa(x)/(\phi \eta \beta)$, where κ is permeability, η is fluid viscosity, ϕ is porosity, and β is the fluid compressibility. x_0 is the location of the fluid injector. $\kappa(x) = \kappa_1$ if $|x| > L_k$, and $\kappa(x) = \kappa_2$ if $|x| < L_k$; also with D_1 and D_2. q is the (constant) fluid mass flux, ρ_f is the fluid density, δ is the Dirac delta function, and $H(t)$ is the Heaviside unit step function. We assume all properties are constants except permeability takes a high value inside the channel (κ_2), and a low value outside (κ_1).

To solve this system, we discretize the domain into a uniform grid and solve using an algorithm developed by *Elsworth and Suckale* [2016]. Supp. Table S5 gives the parameter values we use for solving for pore pressure in the channel. We assume zero-pressure boundary conditions at the top and bottom of the domain, and zero-gradient conditions

at the left and right sides of the domain, and neglect poroelastic effects in this analysis. Supp. Fig. S3 shows the pressure distribution after 100 days and 1000 days.

S3: Impact of limited roughness resolution on rupture size

In the simulator we use, artificially-nucleated earthquakes can propagate at stress levels less than 0.6-0.7, at which most faults in the crust, particularly in intra-cratonic settings, are thought to operate [e.g., *Walsh and Zoback*, 2015] . The reason for this is that on "smooth" faults, i.e. where roughness down to the wavelength of slip is not modeled, strong rate-weakening friction allows rupture propagation at much lower stress levels than static failure.

Fang and Dunham [2013] address this issue in their study, and point out that many laboratory experiments show that fault materials undergo significant weakening at high slip speeds. They postulate that the additional resistance to slip related to the propagation of the rupture around bends in the fault, termed "roughness drag" (τ^{drag}), is responsible for the difference between the low friction measured in the lab and the shear/normal stress ratios implied by more traditional fault studies. They derived an approximate expression for τ^{drag}, given in Eq. 2 in the main text, which depends on fault roughness α as well as the minimum roughness wavelength $\lambda_{\min}$. Their derivation is based on the scaling pointed out by *Dieterich and Smith* [2009]:

$$\tau^{\mathrm{drag}} \propto \frac{\alpha^2 \Delta}{\lambda_{\min}}$$

where Δ is slip. In our simulations, $\Delta/\lambda_{\min} \approx 0.01$, so τ^{drag} ranges from 0.1-10 MPa for $\alpha = 0.001 - 0.01$. However, for lower values of the minimum roughness wavelength τ^{drag} can increase substantially. As *Fang and Dunham* [2013] point out, as the minimum

wavelength approaches the scale of slip, pervasive off-fault yielding is expected to occur, leading to shear over normal stress ratios approximately equal to the internal friction coefficient of the host rock, which may be 0.6-0.8.

Fang and Dunham [2013] estimate that, accounting for roughness down to the scale of slip, the resistance drag stress during slip due to roughness τ^{drag} is on the order of 10 MPa for $\alpha = 0.001$ and could approach the background level for high roughness. As they point out, this could explain the discrepancy between low values of friction observed in laboratory experiments of dynamic friction and classic estimates. Supp. Fig. S12 shows how rupture size changes as the minimum roughness wavelength changes.

In the majority of the simulations shown in this study, the minimum roughness wavelength is 300 m. With this value, $\Delta/\lambda_{\text{min}} \approx 10^{-3}$, so τ^{drag} in our simulations is about a factor of 1000 smaller than expected if roughness on crustal faults scales down to the scale of slip. We conducted a limited number of simulations using roughness wavelengths of 150 and 600 meters to compare to the reference case. Figure S12 shows how the resistance to slip due to roughness drag scales with λ_{min}, roughness α, and slip Δ. S12a shows, for the limited range of λ_{min} we test in our simulations, how the median rupture length (out of 100 simulations) changes for a given stress level and two different roughnesses. S12b shows the theoretical scaling of τ^{drag} with λ_{min}, the vertical lines represent the three values used in plot (a). It is clear that having the computational ability to allow roughness wavelengths down to the meter level would significantly increase the background stress necessary to sustain dynamic rupture.

We also show scatter plots of τ^{drag} versus rupture length in Figure S13. These plots clearly demonstrate the change in rupture size that occurs as the minimum roughness wavelength changes. Note that for these simulations, the fault is the same at wavelengths greater than 600 meters. The additional roughness due to refining $\lambda_{\min}$ does not necessarily contribute to higher stresses, but to stress variations on smaller scales. These variations lead to more plastic yielding from larger strains and also may contribute to increased radiation, both of which dissipate energy from the propagating rupture, and so the overall rupture length tends to end up smaller.

References

Dieterich, J. H., and D. E. Smith (2009), Nonplanar Faults: Mechanics of Slip and Off-fault Damage, *Pure and Applied Geophysics*, *166*(10-11), 1799–1815, doi: 10.1007/s00024-009-0517-y.

Dunham, E. M., D. Belanger, L. Cong, and J. E. Kozdon (2011), Earthquake Ruptures with Strongly Rate-Weakening Friction and Off-Fault Plasticity, Part 1: Planar Faults, *Bulletin of the Seismological Society of America*, *101*(5), 2296–2307, doi: 10.1785/0120100076.

Elsworth, W. C., and J. Suckale (2016), Rapid ice flow rearrangement induced by subglacial drainage in West Antarctica, *Geophysical Research Letters*, *43*(22), 697–11, doi: doi:10.1002/2016GL070430.

Fang, Z., and E. M. Dunham (2013), Additional shear resistance from fault roughness and stress levels on geometrically complex faults, *Journal of Geophysical Research: Solid Earth*, *118*(7), 3642–3654, doi:10.1002/jgrb.50262.

Noda, H., E. M. Dunham, and J. R. Rice (2009), Earthquake ruptures with thermal

weakening and the operation of major faults at low overall stress levels, *Journal of

Geophysical Research*, *114*(B7), B07,302, doi:10.1029/2008JB006143.

Rice, J. R. (1983), Constitutive relations for fault slip and earthquake instabilities, *Pure

and Applied Geophysics PAGEOPH*, *121*(3), 443–475, doi:10.1007/BF02590151.

Walsh, F. I. R., and M. D. Zoback (2015), Oklahoma's recent earthquakes and saltwater

disposal, *Science Advances*, *1*(5), 1–9, doi:10.1126/sciadv.1500195.

Zheng, G., and J. R. Rice (1998), Conditions under which velocity-weakening friction

allows a self-healing versus a cracklike mode of rupture, *Bulletin of the Seismological

Society of America*, *88*(6), 1466–1483.
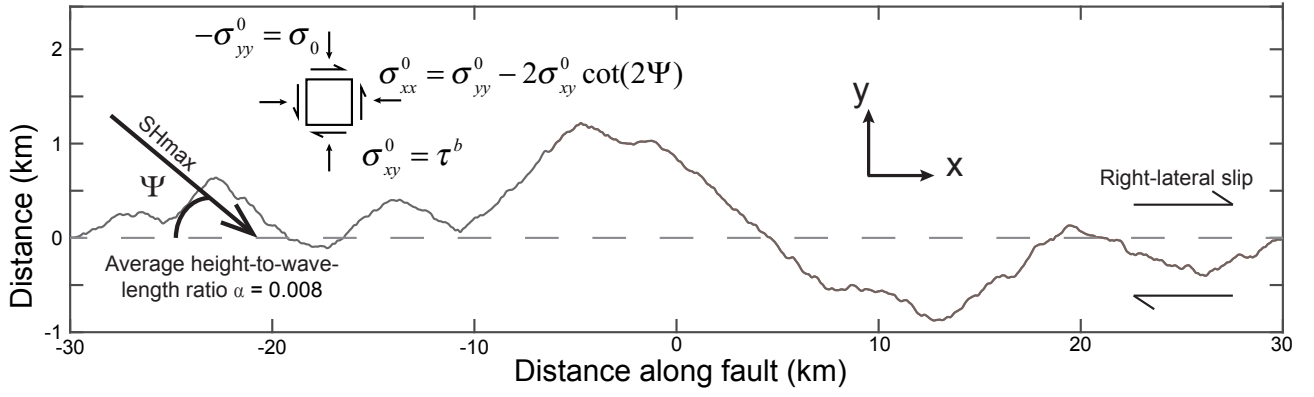
Figure S1.   Diagram showing the basic geometry for the 1-D fault in 2-D medium, including

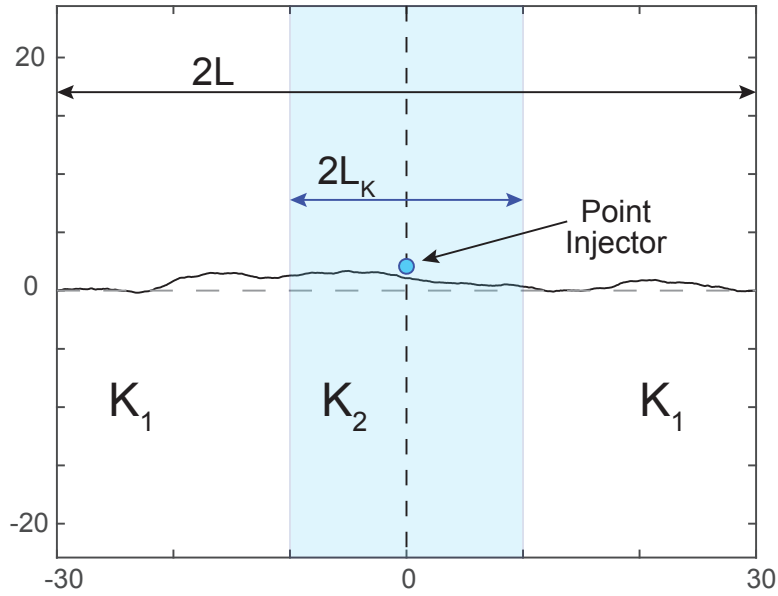the background stress tensor.

Figure S2.   Geometry for the nonuniform permeability pressure model (PM3). Pressure is

computed numerically after 1000 days on injection. The injector is located at $x = 0$, $y = 2$ km.
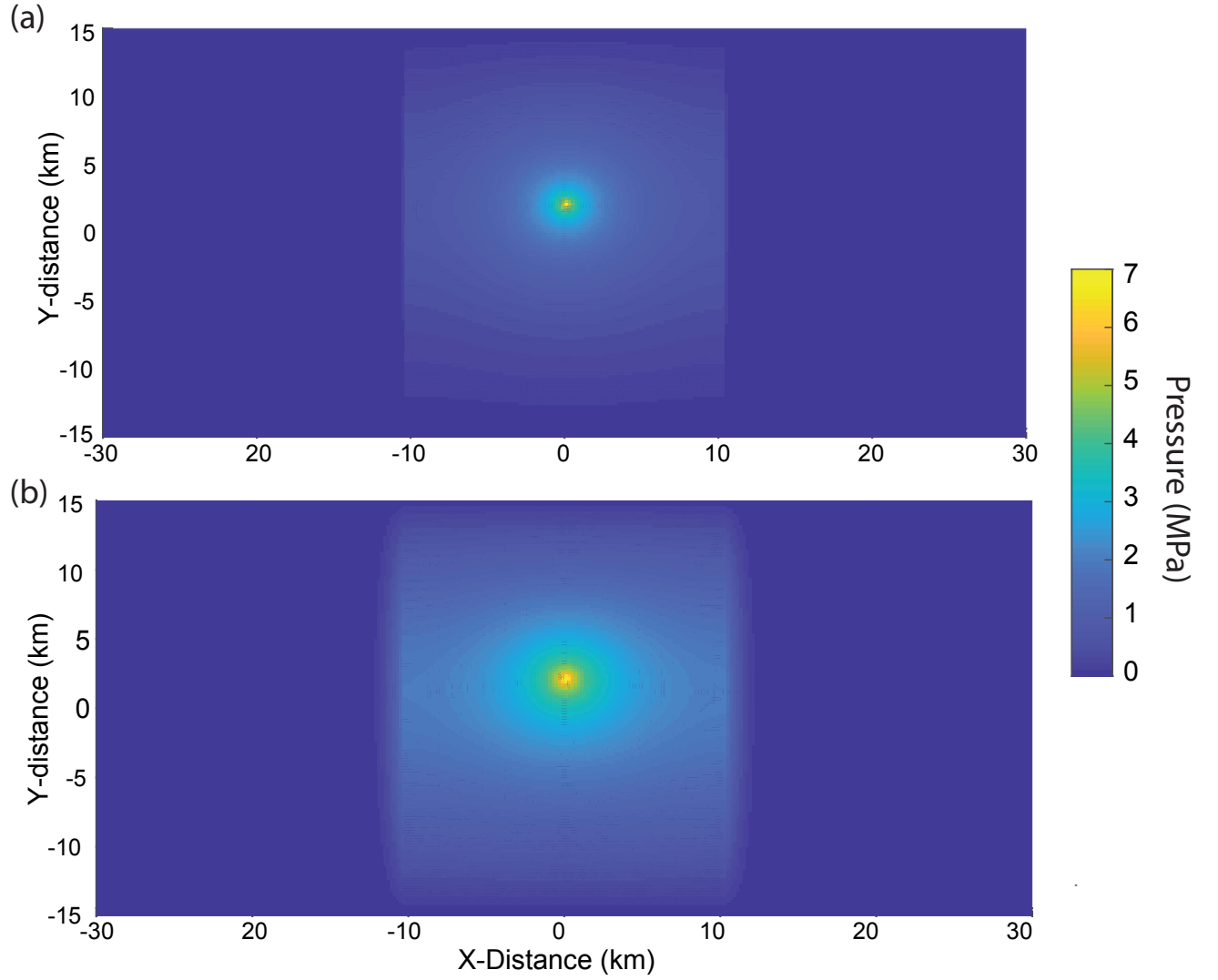
Figure S3. Pressure distribution after (a) 100 and (b) 1000 days of continuous, constant injection. Parameters are as given in Table S5. The horizontal dashed line is the nominal fault location at $y = 0$.
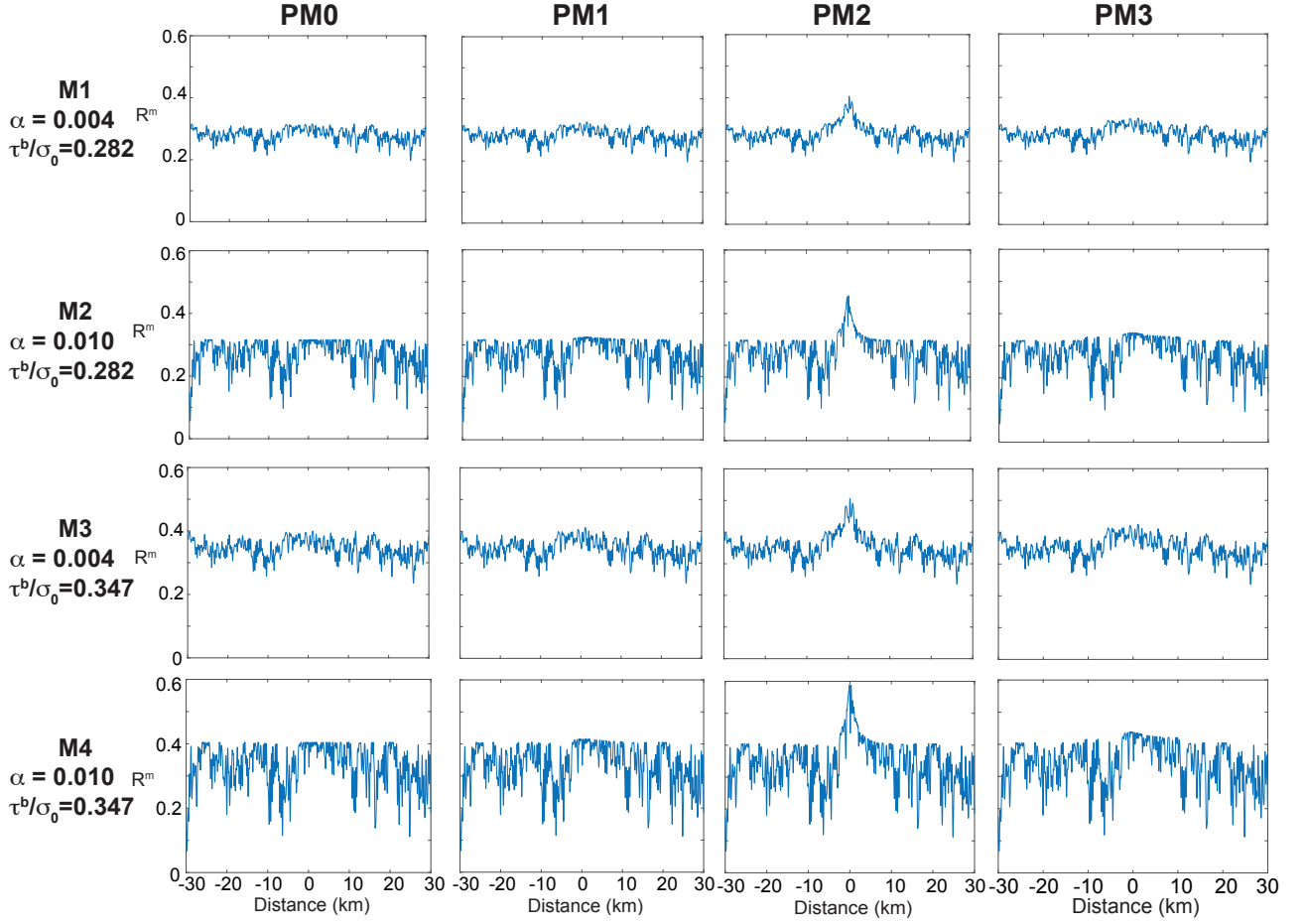
Figure S4.   Initial Shear-to-normal stress ratio for each of the pressure models using four different combinations of background stress ratio and roughness. For comparison, static friction is 0.7.
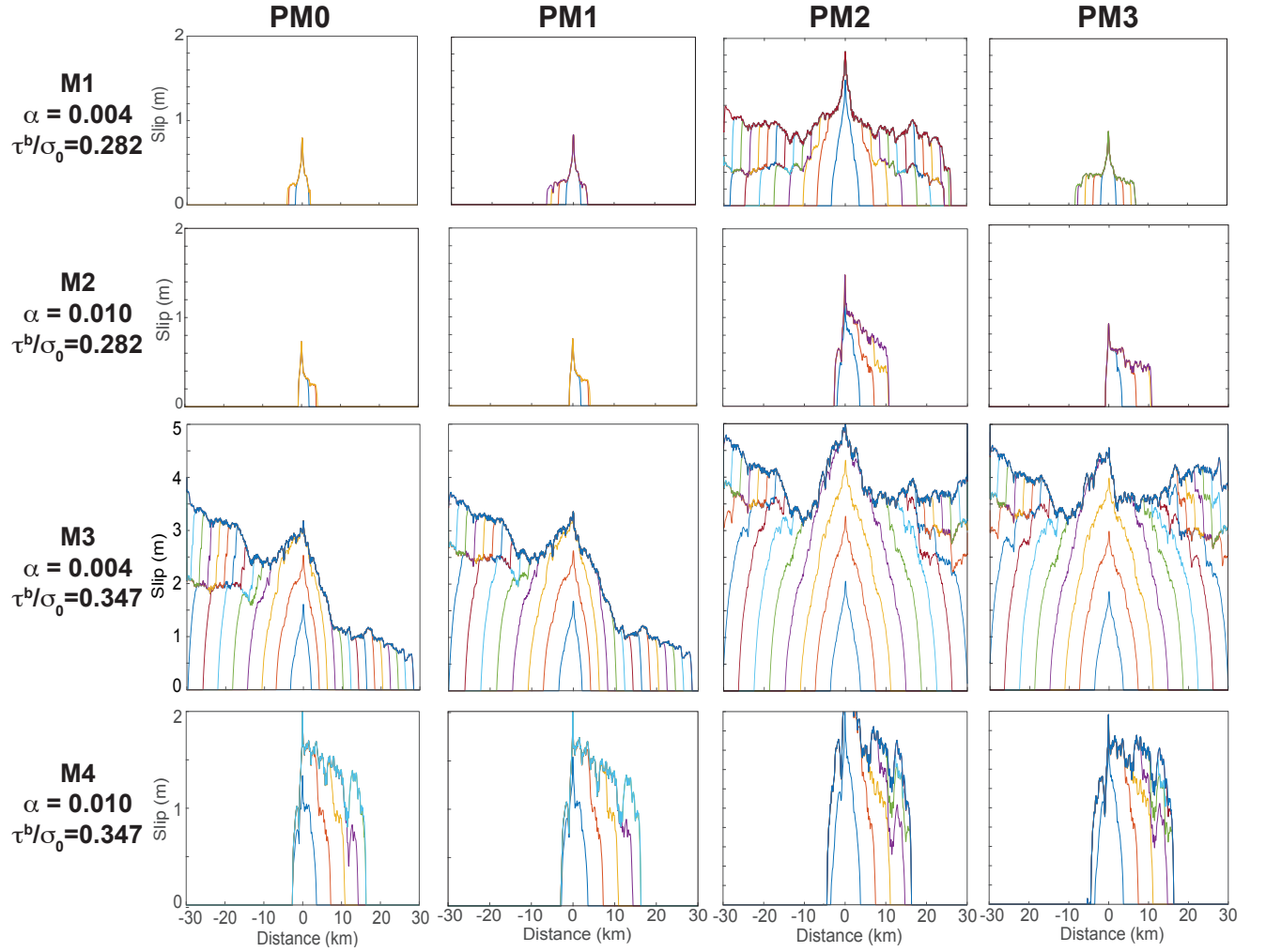
Figure S5. Slip during dynamic rupture for each of the models shown in Supp. Fig. S5. Slip is shown at regular time intervals of 0.7 seconds. Colors are for visual aid only. Note that the vertical scale for M3 ruptures is 5 m, compared to 2 m for the others.
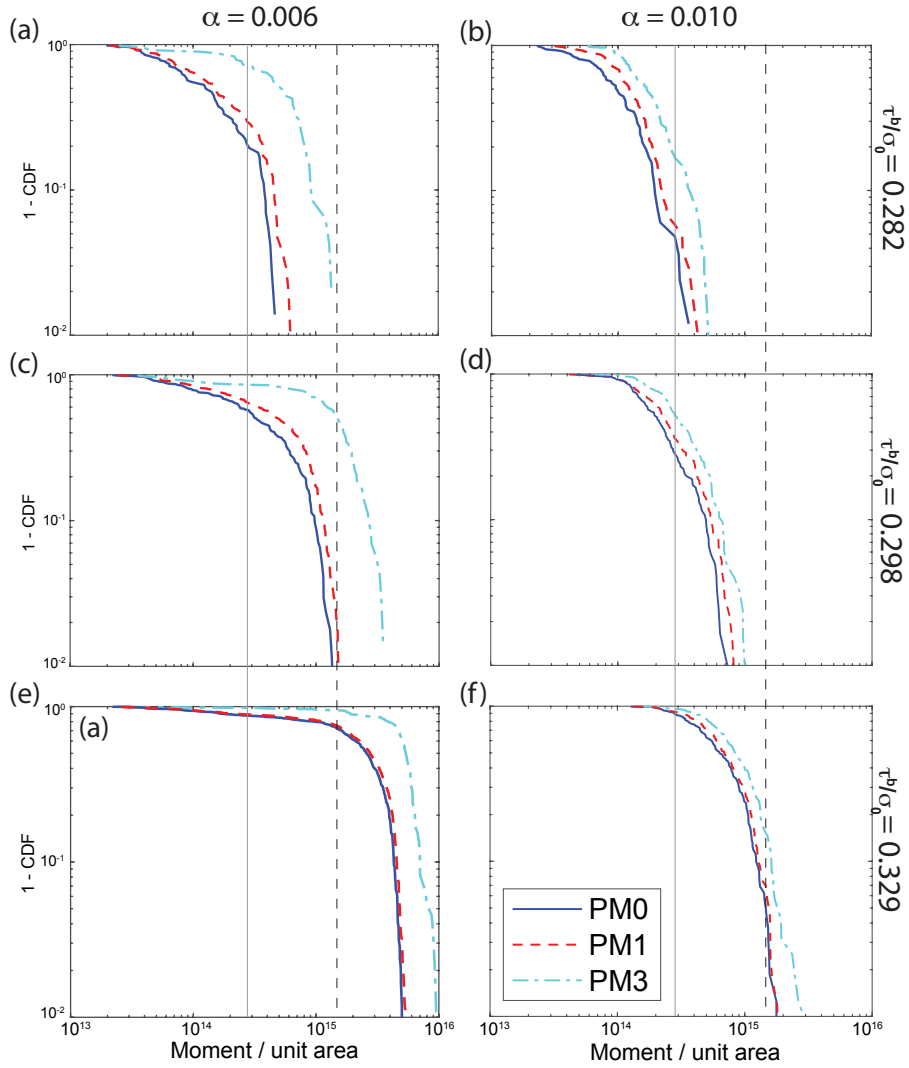
Figure S6.   Frequency-moment distributions for PM0, PM1, and PM3 using a background normal stress equal to 126 MPa. PM2 simulations were not conducted for this normal stress value (126 MPa) because $\sim$ 20 MPa peak pressure perturbation was not thought to be likely at the corresponding depths. Vertical lines show Mmax consistent with Figure 3 in the main text.
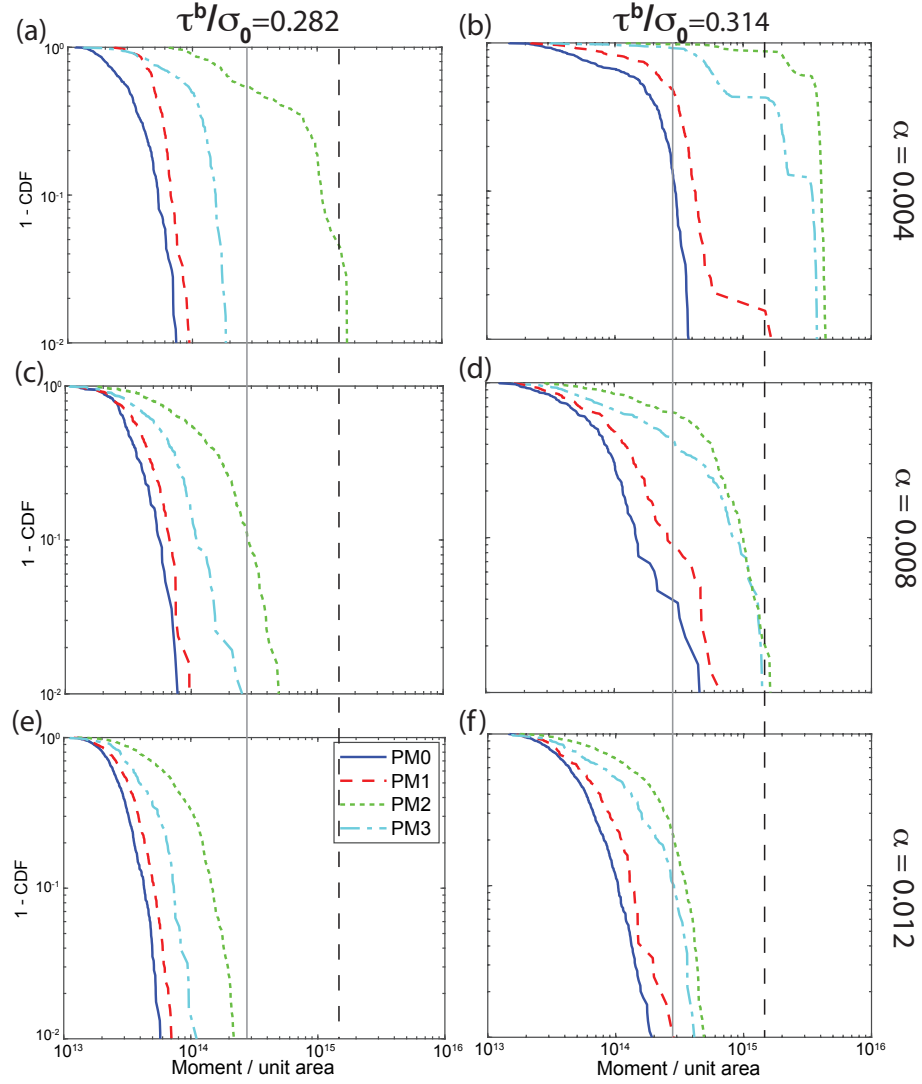
Figure S7. Additional frequency-moment distributions for each of the pressure models using $\sigma_0 = 62$ MPa. (a) is the same as shown in Figure 3 in the main text, but the distributions are normalized to the inverse CDF.
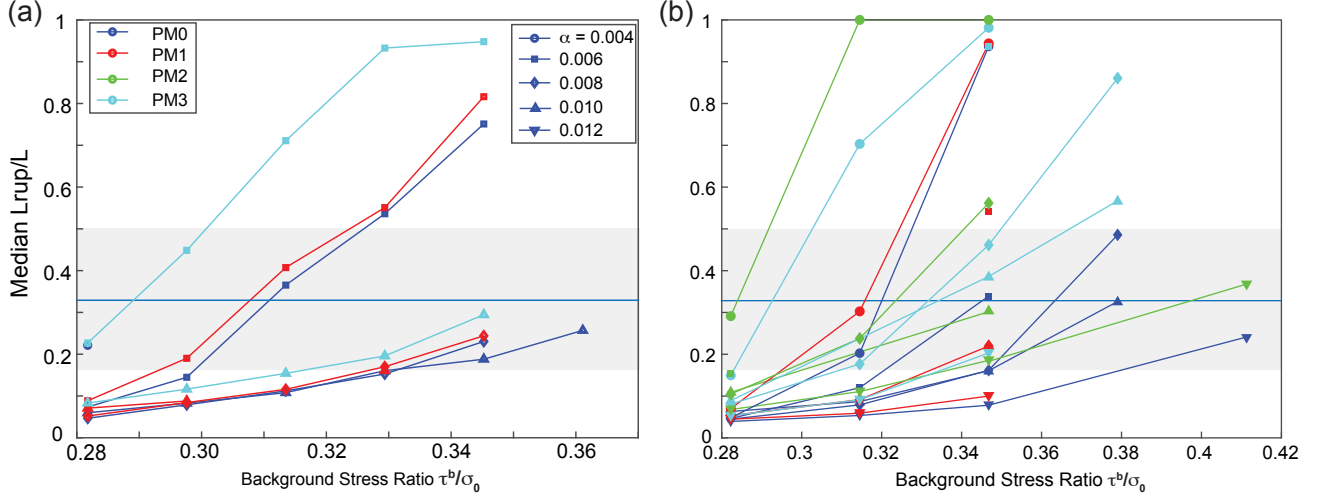
Figure S8. Median normalized rupture length as a function of background stress for (a) high background normal stress (126 MPa) and (b) low background normal stress (62 MPa). Colors represent pressure models and symbol types are roughnesses. The shaded region and solid blue line are the same as in Fig. 1 in the main text, and represent the pressure boundary region for the diffusive models (PM1, PM2) and the width of the high-permeability region for PM3. Each point on the plot represents the median out of 200 simulations.
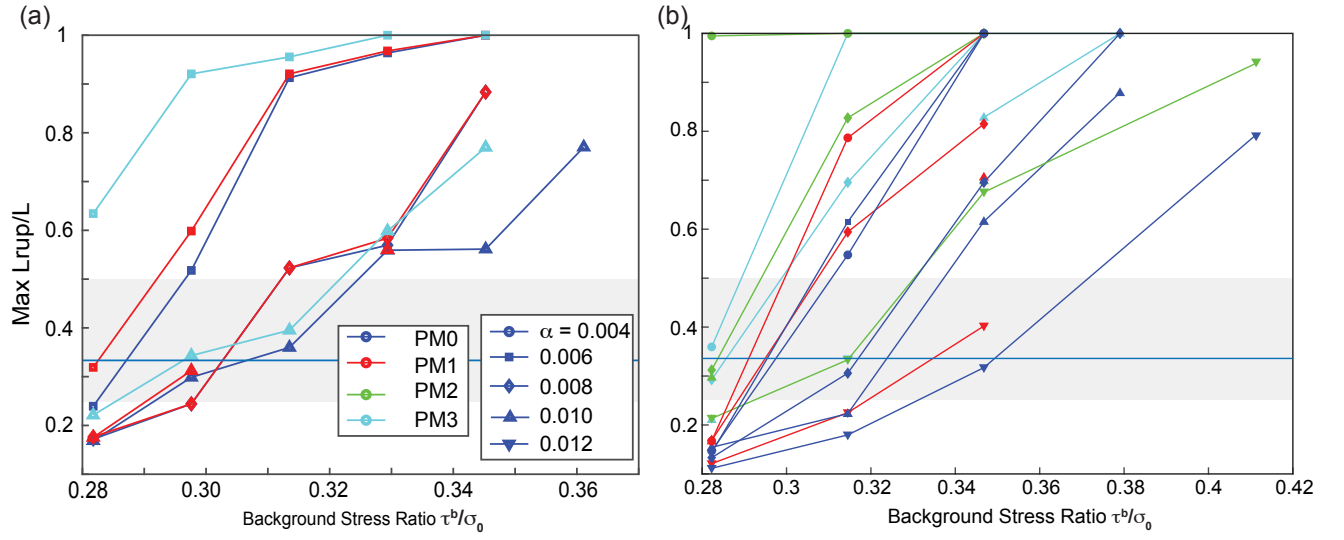
Figure S9.   Same as Fig. S8, but for maximum normalized rupture length. (a) High background normal stress. (b) Low background normal stress.
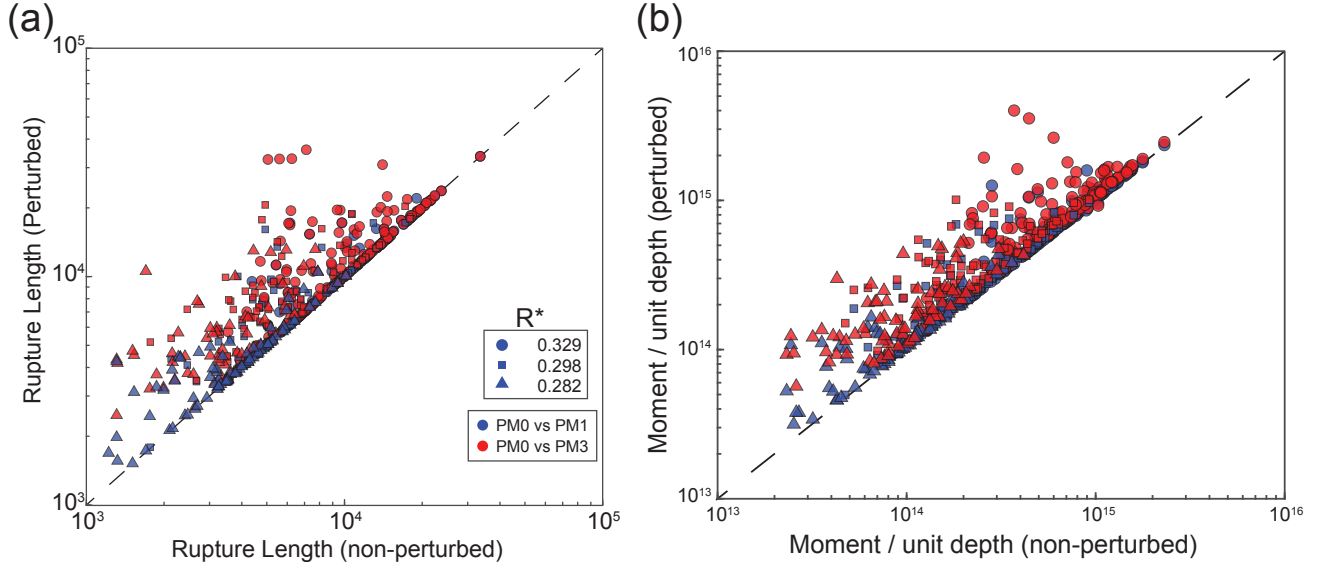
Figure S10. Scatter plots comparing perturbed and non-perturbed event sizes for $\alpha = 0.010$ and $\sigma_0 = 126$ MPa, for (a) rupture length (meters) (b) moment per unit depth (N m /m). Symbol type denotes the background stress level. Blue symbols compare PM0 and PM1, red compare PM0 with PM3. Maximum rupture length is 60 km (6×10^4 m) with corresponding moment approximately 5×10^{15} N m/m.
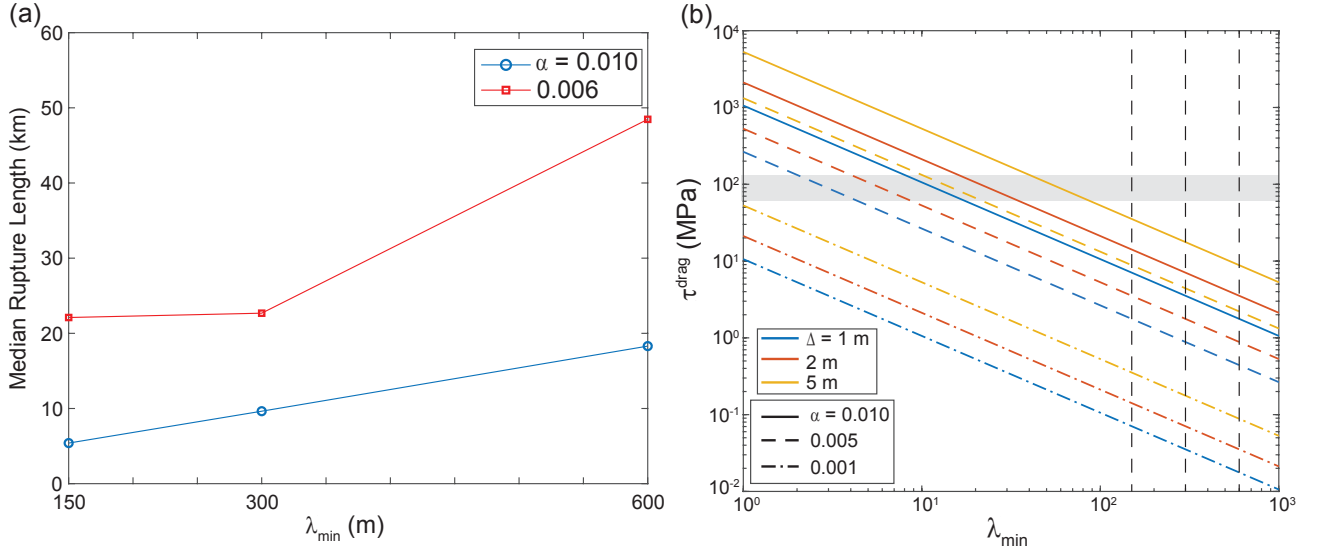
Figure S12.   (a) Median rupture length in km out of 100 simulations, for three different values of λ_{min} and two roughnesses. A simple linear fit gives a slope of approximately 0.03 for $\alpha = 0.010$ and 0.09 for $\alpha = 0.006$. (b) Theoretical scaling of τ^{drag} with λ_{min} for various values of slip Δ and roughnesses. Vertical dashed lines are the values of λ_{min} used in (a). Note that these lines do not take into account the break in scaling resulting from pervasive off-fault damage, discussed in *Fang and Dunham* [2013]. The gray shaded region represents the range of stresses between the high- and low-normal stress cases presented in this study (62 and 126 MPa).
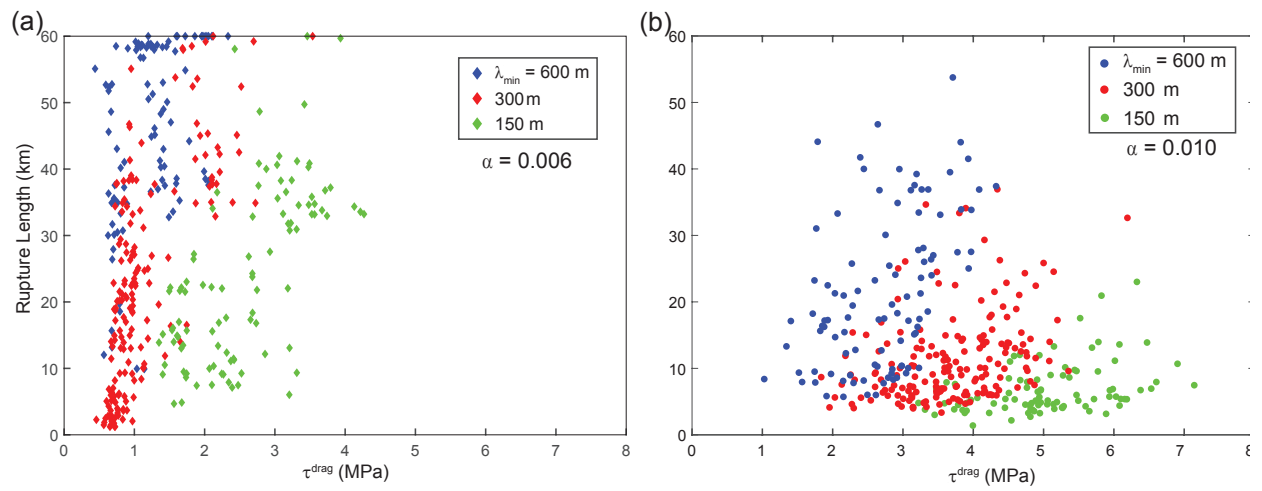
Figure S13.   Scatter plots of rupture length versus τ^{drag} for (a) $\alpha = 0.006$, and (b) $\alpha = 0.010$, for three different values of λ_{min}.

Table S1.   Frictional and stress parameters used in this study and in *Fang and Dunham*

[2013]. These values are for the high normal stress calculations.

Parameter	Value
b	0.02
a	0.016
μ_0	0.7
d_c	0.0857 m
σ^0 (background normal stress)	126 MPa
τ^b (background shear stress)	variable (35.5 - 45.5 MPa)
G (shear modulus)	32.04 GPa
c_s (shear wave speed)	3.464 km/s
ν (Poisson's ratio)	0.25
$\Theta(t = 0)$ (initial state variable)	0.4367
μ (Related to the internal friction coefficient)	$\sin(\arctan(0.7)) = 0.5735$
Ψ (mean fault orientation)	50°

Table S2.   Same as Table S1 but used for the low mean stress simulations with SRW. Values

not repeated here are the same as in Table S1.

Parameter	Value
d_c	0.042 m
σ^0 (background normal stress)	62 MPa
τ^b (background shear stress)	variable (17.5-25.5 MPa)

Table S3.   Parameters for Pressure Model 1.

Parameter	Value
ρ_f	1000 kg/m^3
c	0.36
α	0.4
λ	20 GPa
κ (permeability)	2.24×10^{-15} m^2
G (shear modulus)	32.04 GPa
η (viscosity)	$0.4 \times 10^{-3} Pa - s$
ν (Poisson's ratio)	0.25
q (mass flux)	0.05 m^3/s
B	0.5
λ_u	30 GPa
10-kPa width	19 km
Origin	[0, 2 km]

Table S4. Parameters for Pressure Model 2. Those not given are identical to PM1.

Parameter	Value
c	0.1
q (mass flux)	0.28 m^3/s
10-kPa half-width	12.5 km
Stretch	Y-direction, 4x

Table S5. Parameter values used for the three-zone pressure diffusion problem.

Parameter	Value
κ_1	10^{-16} m^2
κ_2	10^{-13} m^2
ρ_f (Fluid density)	1000 kg/m^3
p_0 (Initial pressure)	0 MPa
η (Fluid viscosity)	4×10^{-4} Pa s
β (Fluid compressibility)	3.2×10^{-10} 1/Pa
ϕ (porosity)	0.12
q (Mass injection rate)	2 kg/sec
L	30 km
L_k	10 km
y_0 (Injector Location)	2 km
h	200 m
Δt	1000 sec
$D_1 = \kappa_1/(\phi\beta\eta)$	0.0065 m^2/s
$D_2 = \kappa_2/(\phi\beta\eta)$	6.5 m^2/s